Micellization Kinetics of Block Copolymers in Selective Solvent

Chikako Honda,* Yuki Hasegawa, and Rieko Hirunuma

Showa College of Pharmaceutical Sciences, Higashitamagawagakuen 3-3165, Machida-shi, Tokyo 194, Japan

Takuhei Nose

Department of Polymer Chemistry, Tokyo Institute of Technology, Ookayama, Meguro-ku, Tokyo 152, Japan

Received May 9, 1994; Revised Manuscript Received September 14, 1994[⊗]

ABSTRACT: Micellization kinetics of poly(α-methylstyrene)-*block*-poly(vinylphenethyl alcohol) (PαMS-*b*-PVPA) in selective solvent, benzyl alcohol (BA), was investigated by time-resolved static and dynamic light scattering. Time evolution of apparent molecular weight M_{wapp} and radius of gyration R_{gapp} were measured for two (PαMS-*b*-PVPA)s (KT-326 and KT-327) of different block compositions in the course of micellization after quenching from the unimer region to the micelle region. The micellization was found to proceed stepwise by fast and slow processes. Observed features of time variation of M_{wapp} and R_{gapp} led to the following conclusions for the micellization processes. In the fast first process, quick association of unimers resulted in the birth of quasi-equilibrium micelles and an increase of the number of quasi-equilibrium micelles dominated over growth of the micelle size. The slow second process of approaching the final equilibrium state primarily proceeded by growth of the micelle size, with accompanying decomposition of the quasi-equilibrium micelles and with a gradual decrease of the micelle number. The time evolution of M_{wapp} was approximately described by an exponential equation with two time constants of the first and second processes. The time constant τ_1 of the first process depended on the polymer concentration strongly, whereas the time constant τ_2 of the second process was almost independent of the concentration. In the case of KT-327 with longer core chains of PVPA block, the value of τ_1 ranged from 0.1 to 1 h, and the value of τ_2 was several tens of hours. KT-326 had much longer τ_1 by about 10^3 times than τ_1 of KT-327. Both τ_1 and τ_2 of KT-327 decreased with increasing temperature.

Micellization of block copolymers in selective solvent has extensively been studied theoretically and experimentally.[1−25] However, very few studies on the kinetics of the micellization have been reported for polymeric systems.[14−16,23,24] Considerable efforts have been devoted to studies of micellization kinetics for surface active agents of low molecular weight substances near the association equilibrium.[26−38] The association or dissociation from one equilibrium to another equilibrium state takes place essentially by two processes. The faster process is associated with redistribution of the association number of respective micelles with no change of the total number of micelles, while the slower process is to approach the final equilibrium by micelle formation and decomposition with a change in the total number of micelles. Figure 1 schematically illustrates variation of the association number distribution in the two relaxation processes.[29] This idea was theoretically described for the first time by Aniansson and Wall[27] to interpret experimental observations with chemical relaxation techniques and have been confirmed by many experiments[26,28,30,31,33−35,37] and discussed theoretically to a large extent.[11,29,32,36] For block copolymers, the relaxation time for a polymer chain escaping from the micelle, which may be a rate-determining process in the slow process mentioned above, has theoretically been discussed on the basis of scaling analysis.[15,16,20] Tuzar and co-workers[1,14] followed the processes of micelle formation and decomposition of block copolymers by means of the stopped-flow method with light scattering and found that the relaxation time of micellization was of the order of 10 ms, while the decomposition occurred much more quickly than the micellization. Mattice et al.[24] made a computer simulation for micellization of

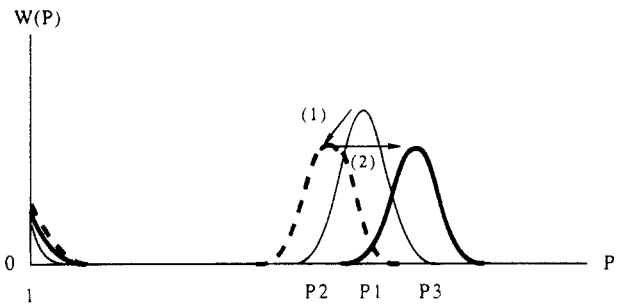

Figure 1. Schematic presentation of redistribution of association number in the relaxation near equilibrium according to the Aniansson−Wall (A−W) theory.[27,29] Distribution function $W(P)$ expresses the weight fraction of associates having association number P. (Thin solid line) Initial; (dashed line) after the fast process; (heavy solid line) final. The fast process (1) is the decrease of the average association number from P_1 of initially formed micelles to P_2 of the quasi-equilibrium micelles with no change in the number of the micelles but with increasing unimer−number corresponding to that decrease. The second process (2) followed by the fast process is the growth of each micelle to approach the final equilibrium size (average association number P_3), accompanying a decrease of the micelle number by micelle decomposition.

block copolymers, suggesting the presence of two processes with different time scales. To our knowledge, no detailed experimental data of micellization kinetics have been reported for polymeric systems as yet.

In general, the micellization process is too fast to be easily followed experimentally, when it takes place far away from the critical micelle concentration or temperature. In this study, we selected experimental conditions near the critical micellization to investigate micellization kinetics of block copolymers in selective solvent by means of static and dynamic light scattering. The system used here was poly(α-methylstyrene)-*block*-poly(vinylphenethyl alcohol) in benzyl alcohol, which

[⊗] Abstract published in *Advance ACS Abstracts,* November 15, 1994.

0024-9297/94/2227-7660$04.50/0

Table 1. Molecular Weight and Composition of Block Copolymers

sample code	$M_{P\alpha MS}$, $\times 10^{-4}$	M_{PVPA}, $\times 10^{-4}$	M_{total}, $\times 10^{-4}$	ϕ_{PVPA}[a]
KT-326	7.0	1.1	8.1	0.11
KT-327	11.3	1.23	12.5	0.08

[a] ϕ_{PVPA}; PVPA composition in fractional degree of polymerization.

has the critical micelle temperature a little above room temperature. The micellization process was so slow that the process could be observed by time-resolved light scattering measurements. Angular dependence of integrated scattered-light intensity and autocorrelation function of the intensity were measured in the course of micellization after quenching from the unimer region to the micelle region. Apparent molecular weight and radius of gyration obtained by light scattering give different averages of association number and size of the colloid particles in the solution, respectively, which enables us to tell which process dominates over the other in the process, the size growth or the association number increase. Two processes with different rates, similar to those of low molecular weight surfactants, have been observed in the present polymeric systems. The micellization rates for these processes are discussed as a function of polymer concentration for two copolymers with different block compositions.

Experimental Section

Materials. Poly(α-methylstyrene)-*block*-poly(*p*-vinylphenethyl alcohol)s (PαMS-*b*-PVPA) were anionically polymerized ones with the sample codes KT-327 and KT-326,[39] of which characteristics are listed in Table 1. Molecular weight distribution indices M_w/M_n were around 1.1.

Benzyl alcohol (BA), purchased, was used without distillation. BA is a thermodynamically good solvent to PVPA, and a nonsolvent to PαMS, so that the PαMS block may aggregate to form a core and the PVPA block may make corona when the copolymer forms a micelle. In fact, it was found in our previous work[40] that KT-327 formed crew-cut star-shaped micelles in *m*-chlorobenzyl alcohol.

Light Scattering Measurements. Static and dynamic light scatterings were performed by using a DLS-700 apparatus manufactured by Ohtsuka Electronic Co. Ltd., with an Ar ion laser operated at 488 nm as light source.

The solvent was optically purified by a Teflon filter with the nominal pore size of 0.2 μm. Stock solutions were prepared by dissolving the block copolymers in BA, keeping the solutions at 55–60 °C for 2–3 h and optically purifying through a Teflon filter with the nominal pore size of 0.45 μm. The stock solutions were diluted by adding the purified solvent in a dust-free optical cell to make the sample solution with desired concentration ranging from 6×10^{-4} to 1.5×10^{-3} g (g of solution)$^{-1}$ for KT-326 and from 2×10^{-4} to 8×10^{-4} g (g of solution)$^{-1}$ for KT-327. Subsequently, the optical cell was flame sealed under mild vacuum.

Integrated intensity of scattered light was measured as a function of scattering angle θ ranging from 30° to 145°. It took about 4 min to measure a set of data, which was much shorter than the time scale of micellization, so that no correction of time lag was needed.

Excess Rayleigh ratio $\Delta R(\theta)$ was calculated from the measured excess scattered intensity using the intensity of benzene as standard with the Rayleigh ratio of benzene being 3.405×10^{-5} cm^{-1} at 25 °C.[41]

Since, in the time-resolved measurement, the conventional analysis using the extrapolation to the dilute limit was not available, we evaluated apparent molecular weight M_{wapp} and apparent radius of gyration R_{gapp} without the extrapolation, which are defined as

$$M_{wapp} = \Delta R(0)/Kc \tag{1}$$

$$R_{gapp} = \frac{(\text{initial slope})3\lambda_0^2 M_{wapp}}{16\pi^2 n^2} \tag{2}$$

where c is the polymer concentration in g mL^{-1} and K is the optical constant defined by $K = 4\pi^2 n^2 (dn/dc)^2/\lambda^4 N_A$, with n, λ_0, and N_A being the refractive index, the wavelength of the incident beam, and the Avogadro constant, respectively. $Kc/\Delta R(0)$ and (initial slope) are the intercept and the initial slope of the Zimm plot, $Kc/\Delta R(\theta)$ vs $\sin^2(\theta/2)$, at finite concentrations. The refractive index increment (dn/dc) was measured by a differential refractometer, DRM-1020, of Ohtsuka Electronic Co. Ltd., with the wavelength $\lambda_0 = 488$ nm at 30 °C. Measured (dn/dc) for PαMS was 0.0716 mL g^{-1}. The (dn/dc) of PVPA in BA was estimated to be 0.0249 mL g^{-1} from the dn/dc of PVPA in *m*-chlorobenzyl alcohol (CBA)[40] and refractive index difference between BA and CBA. Values of (dn/dc) for the block copolymers were calculated, on the basis of refractive index additivity, from these (dn/dc) values to be 0.0653 and 0.0671 mL g^{-1} for KT-326 and KT-327, respectively. Their temperature dependences were so small in the experimental temperature range (from 15 to 45 °C) that they were neglected in the data analysis. Because of the small content and the small (dn/dc) value of PVPA, the obtained R_{gapp} can be regarded as the $\langle R_g^2 \rangle$ of PαMS part of the block copolymer micelle.

Accumulation time for measuring the autocorrelation function $g^{(2)}(\tau)$ of the scattered light intensity ranged from 5 to 10 min, and the measurements were carried out for KT-326 solutions in the micellization process of time t being longer than 30 min after quenching, where change in properties of the solution during the data-taking time could be ignored. The obtained $g^{(2)}(\tau)$ was transformed to the correlation function $g^{(1)}(\tau)$ of the electric field of scattered light by the following equation for the self-beat method.

$$g^{(2)}(\tau) = A(1 + B|g^{(1)}(\tau)|^2) \tag{3}$$

A and B are constants. The correlation function $g^{(1)}(\tau)$ was analyzed by the cumulant method.[42] By the nonlinear least-squares fitting to the cumulant expansion

$$|g^{(1)}(\tau)| = \exp(-\bar{\Gamma}\tau + (\mu_2/2)\tau^2 - \ldots) \tag{4}$$

we evaluated the average decay rate $\bar{\Gamma}$, the second cumulant μ_2, and the particle size distribution index, $\mu_2/\bar{\Gamma}^2$. The diffusion coefficient D was obtained by the relation, $\bar{\Gamma} = Dq^2$. The hydrodynamic radius R_h was calculated with the Stokes–Einstein equation

$$R_h = k_B T/6\pi\eta D \tag{5}$$

where k_B, T, and η are the Boltzmann constant, the absolute temperature, and the solvent viscosity, respectively. η was measured by a Ubbelohde type viscometer as a function of temperature. Similarly to the static properties, since the extrapolation to zero concentration could not be made, we evaluated the hydrodynamic radius without the extrapolation, which was here referred to as apparent hydrodynamic radius R_{happ}.

KT-326 and KT-327 started forming micelles around 24 and 50 °C, respectively, under cooling at the rate of 2 °C/min, as shown in Figure 2. For KT-326, we first kept the solution at 40 °C to completely decompose the micelles into the unimers and then quenched to 15 °C to carry out light scattering measurements as a function of time t. For KT-327, the initial temperature was selected to be 60 °C and the micellization was observed at 15, 24, 35, and 45 °C.

Results and Discussion

Micellization of KT-327. Figure 3 shows the time dependence of M_{wapp} and R_{gapp} in log–log scale for various temperatures at the polymer concentration $c = 4.29 \times 10^{-4}$ g (g of solution)$^{-1}$. It took a very long time

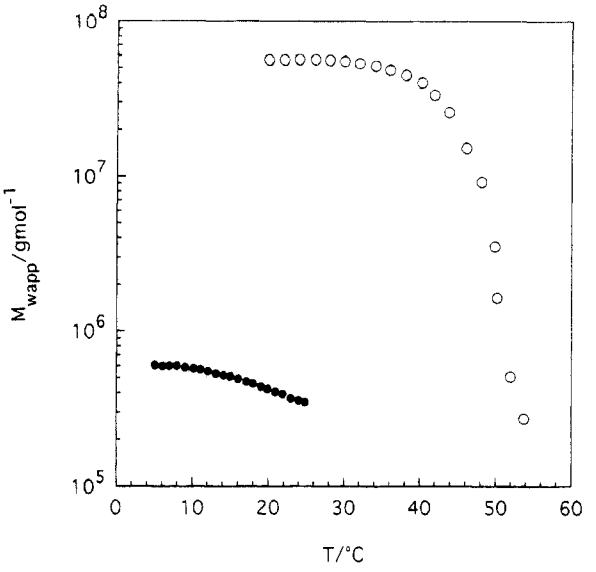

Figure 2. Change of M_{wapp} with decreasing temperature T for KT-326 (●) and KT-327 (○).

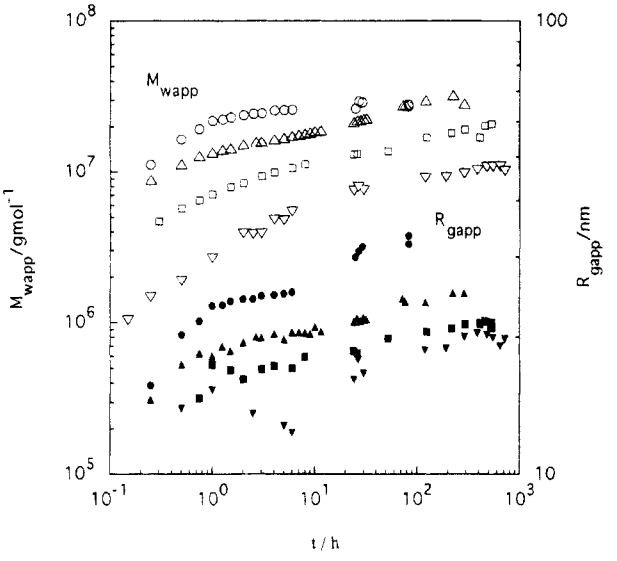

Figure 3. Time evolution of M_{wapp} and R_{gapp} after quenching KT-327 solution from 60 °C to different temperatures. M_{wapp}: 45 °C (○); 35 °C (△); 24 °C (□); 15 °C (▽). R_{gapp}: 45 °C (●); 35 °C (▲); 24 °C (■); 15 °C (▼). Concentration was 4.29 × 10^{-4} g (g of solution)$^{-1}$.

for the micelle to reach an equilibrium size. At earlier time, M_{wapp} increased relatively quickly, seemed to level off tentatively, and then gradually increased again. That is, the micellization appeared to proceed in two steps. At lower temperatures, the transition from the first process to the second process occurred later; in other words, the log M_{wapp}–log t curve shifts towards longer time as the temperature decreases. This may imply that the micellization process was slower at lower temperatures. One can see similar behavior in the R_{gapp}.

Figure 4 represents concentration dependence of the log M_{wapp}–log t relation at the fixed temperature 35 °C. The stepwise micellization is seen more clearly. The growth rate of the first faster process strongly depends on the polymer concentration, whereas that of the second slower process was almost independent of the concentration. Looking at the data closely, one can notice that R_{gapp} levels off earlier than M_{wapp} does in the first process, while parallel growth of R_{gapp} and M_{wapp} was found in the second process. This trend can

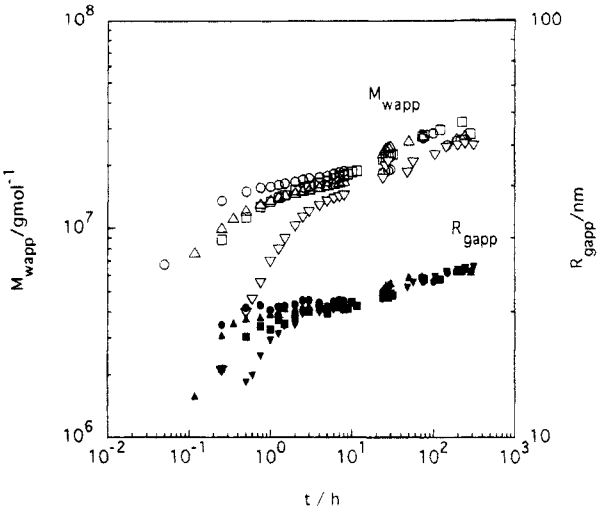

Figure 4. Time evolution of M_{app} and R_{gapp} for KT-327 solutions of various concentrations at 35 °C. M_{wapp}: 8.142 × 10^{-4} g (g of solution)$^{-1}$ (○); 5.934 × 10^{-4} g (g of solution)$^{-1}$ (△); 4.287 × 10^{-4} g (g of solution)$^{-1}$ (□); 2.109 × 10^{-4} g (g of solution)$^{-1}$ (▽). R_{gapp}: 8.142 × 10^{-4} g (g of solution)$^{-1}$ (●); 5.934 × 10^{-4} g (g of solution)$^{-1}$ (▲); 4.287 × 10^{-4} g (g of solution)$^{-1}$ (■); 2.109 × 10^{-4} g (g of solution)$^{-1}$ (▼).

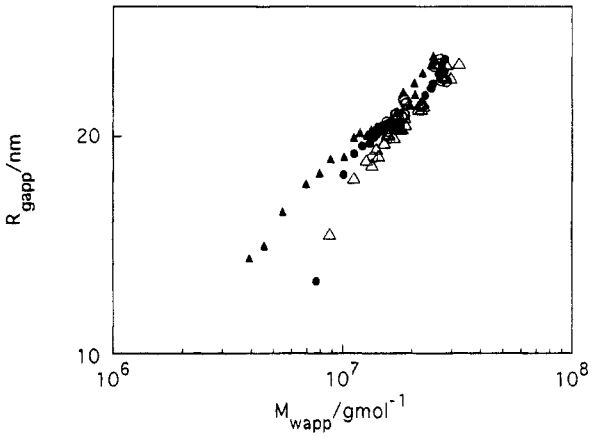

Figure 5. Relationship between R_{gapp} and M_{wapp} for KT-327 solutions of various concentrations at 35 °C. 8.142 × 10^{-4} g (g of solution)$^{-1}$ (○); 5.934 × 10^{-4} g (g of solution)$^{-1}$ (●); 4.287 × 10^{-4} g (g of solution)$^{-1}$ (△); 2.109 × 10^{-4} g (g of solution)$^{-1}$ (▲).

also be seen in the data of Figure 3. To show this behavior more clearly, log R_{gapp} was plotted against log M_{wapp} in Figure 5.

This leads to the following conclusions on the micellization processes. The advancement of R_{gapp} growth over M_{wapp} growth implies that the dominant process is increment of the number of micelles with similar sizes, i.e., micelle fraction growth, as demonstrated in the Appendix. Therefore, in the first process, formation of each micelle from unimers proceeds very quickly, resulting in the increase of the micelle number observed as the dominant process. On the other hand, the parallel increases of R_{gapp} and M_{wapp} suggest that, in the second process, growth of the micelle size takes place very slowly with accompanying decrease of the number of micelles and almost no change of the micelle fraction (see the Appendix).

Micellization of KT-326. In Figure 6 are shown log–log plots of M_{wapp}, R_{gapp}, and R_{happ} against time t. The plots of log M_{wapp} vs log t are of S-shape and showed no level-off at intermediate stage and no stepwise growth, in contrast to those of KT-327. The growth rate decreases with decreasing concentration; i.e., the plots

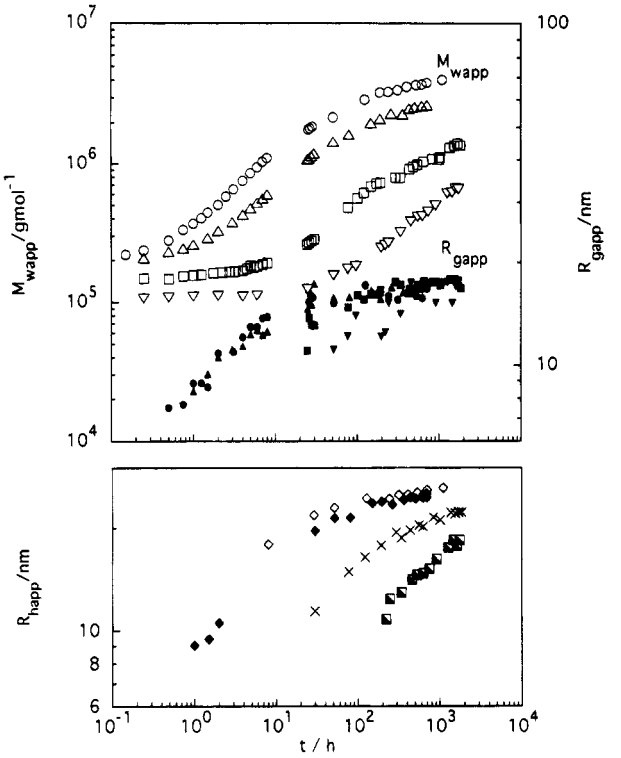

Figure 6. Time evolution of M_{wapp}, R_{gapp}, and R_{happ} for KT-326 solutions of various concentrations at 15 °C. M_{wapp}: 1.517×10^{-3} g (g of solution)$^{-1}$ (○); 1.200×10^{-3} g (g of solution)$^{-1}$ (△); 0.808×10^{-3} g (g of solution)$^{-1}$ (□); 0.601×10^{-3} g (g of solution)$^{-1}$ (▽). R_{gapp}: 1.517×10^{-3} g (g of solution)$^{-1}$ (●); 1.200×10^{-3} g (g of solution)$^{-1}$ (▲); 0.808×10^{-3} g (g of solution)$^{-1}$ (■); 0.601×10^{-3} g (g of solution)$^{-1}$ (▼). R_{happ}: 1.517×10^{-3} g (g of solution)$^{-1}$ (◇); 1.200×10^{-3} g (g of solution)$^{-1}$ (◆); 0.808×10^{-3} g (g of solution)$^{-1}$ (×); 0.601×10^{-3} g (g of solution)$^{-1}$ (◪).

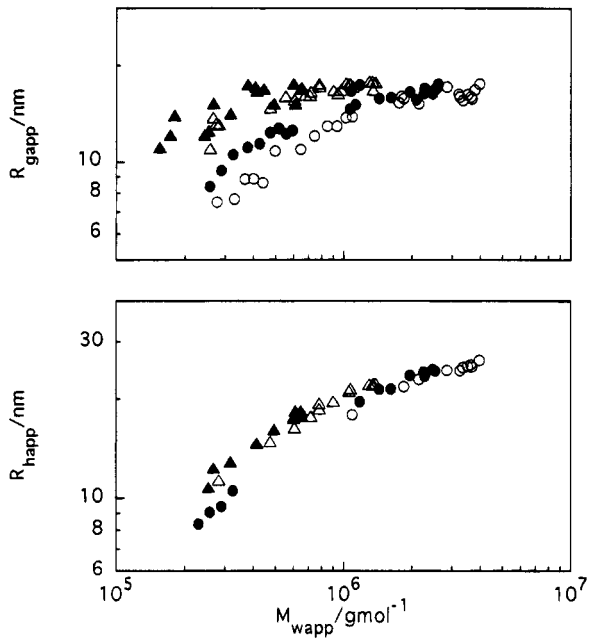

Figure 7. Relationship of R_{gapp} and R_{happ} vs M_{wapp} for KT-326 solutions of various concentrations at 15 °C. Concentration: 1.517×10^{-3} g (g of solution)$^{-1}$ (○); 1.200×10^{-3} g (g of solution)$^{-1}$ (●); 0.808×10^{-3} g (g of solution)$^{-1}$ (△); 0.601×10^{-3} g (g of solution)$^{-1}$ (▲).

shift toward longer time as the concentration decreases. The characteristic difference between M_{wapp} growth and R_{gapp} growth can be noted, which is also represented by log–log plots of R_{gapp} vs M_{wapp} in Figure 7. Change of R_{gapp} almost leveled off in the late stage, while M_{wapp} was still increasing. This advanced growth of R_{gapp} shows the micelle fraction growth dominating over the micelle size growth. Similar behavior of R_{happ} also supports these results (cf. the Appendix). Comparing these results with those of KT-327, one can notice that the process observed in KT-326 corresponds to the earlier stage of the first process observed in KT-327. Characteristic features of the first process are more clearly seen in this case.

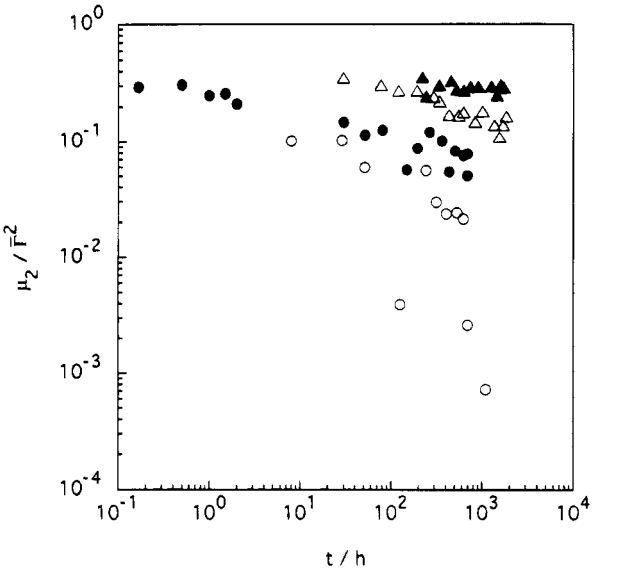

Figure 8. Particle size distribution indices, $\mu_2/\bar{\Gamma}^2$ as functions of time and concentration in KT-326 at 15 °C. The concentrations were 1.517×10^{-3} g (g of solution)$^{-1}$ (○), 1.200×10^{-3} g (g of solution)$^{-1}$ (●), 0.808×10^{-3} g (g of solution)$^{-1}$ (△), and 0.601×10^{-3} g (g of solution)$^{-1}$ (▲).

The micellization observed as the first process is due to increasing micelle number with an almost fixed micelle size; in other words, the growth rate of micelles reaching quasi-equilibrium size is quite high compared with the birth rate of new micelles. Consequently, the particle size distribution of the whole system becomes narrower as the micellization proceeds with increasing micelle fraction. This was consistent with results of the particle size distribution index $\mu_2/\bar{\Gamma}^2$, as shown in Figure 8.

In the first process, as the polymer concentration increases, the birth rate of new micelles becomes higher, especially at the beginning of the micellization, and closer to the rate of size growth from unimers and oligomers. This may lead to the fact that the R_{gapp}–M_{wapp} plots shift M_{wapp} to the larger side with increasing concentration at earlier stage.

Decomposition of the Micelles. Micelles of KT-327 formed by leaving them at 35 °C for 170 h decomposed within 10 min at 50 °C. Decomposition of KT-326 micelles was slower than that of KT-327 micelles and could be followed by light scattering. Figure 9 shows the time dependence of M_{wapp} and R_{gapp} after temperature jumps. R_{gapp} held the initial value for a certain time interval while M_{wapp} was decreasing. Figure 10 of log M_{wapp} vs R_{gapp} plots shows this feature more clearly. This result implies that the decomposition of each micelle is very fast once it starts, and the decrease of the number of micelles is the process observed. The decomposition process corresponds to a reverse process of the first process of micellization. Comparing Figure 9 with Figure 6, one can see that the decomposition process is much faster than the first micellization process. We do not intend to discuss

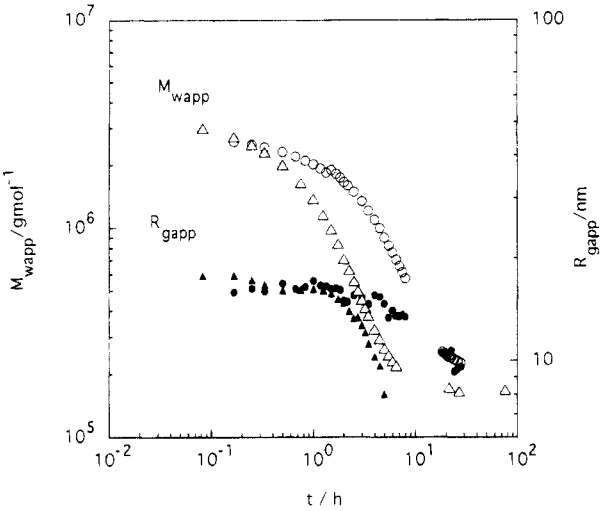

Figure 9. Changes of M_{wapp} and R_{gapp} with time in decomposition of KT-326 micelles after heating from 15 to 30 and 35 °C. M_{wapp}: 30 °C (○); 35 °C (△). R_{gapp}: 30 °C (●); 35 °C (▲).

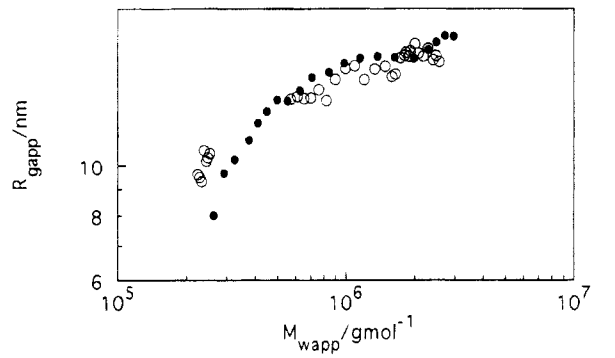

Figure 10. Relationship of R_{gapp} vs M_{wapp} in decomposition of KT-326 micelles after heating from 15 to 30 (○) and 35 °C (●).

details of the decomposition here. Details of decomposition behavior will be presented elsewhere with the kinetics of micelle formation and decomposition by temperature jumps within the temperature region of micelle forming.

Quantitative Analysis for Time Constants of the Two Processes. To evaluate representative time constants for the first and second processes, the growth of M_{wapp} was approximated by an exponential function with a single relaxation time for each process. That is

$$M_{wapp} = M_u + (M_m - M_u)[1 - m_1 \exp(-t/\tau_1) - (1 - m_1)\exp(-t/\tau_2)] \quad (6)$$

with $\tau_1 < \tau_2$. Constants M_u and M_m correspond to molecular weights of a unimer and an equilibrium micelle, respectively, and m_1 is the fractional amplitude of the first process. $M_m m_1$ is the molecular weight of the quasi-equilibrium micelle formed in the first process according to the present interpretation. In describing the results of KT-326, considering that we observed the first process only ($m_1 = 1$), we put, instead of eq 6

$$M_{wapp} = M_u + (M_m - M_u)[1 - \exp(-t/\tau_1)] \quad (7)$$

Time constants τ_1 and τ_2 along with the parameters $M_m - M_u$ and m_1 were obtained by the least-squares fitting to eqs 6 and 7. Examples of fitting curves with the data are shown in Figure 11. In most cases, M_{wapp} changes more gradually than the calculated curves by the single-exponential description. However, the fittings were

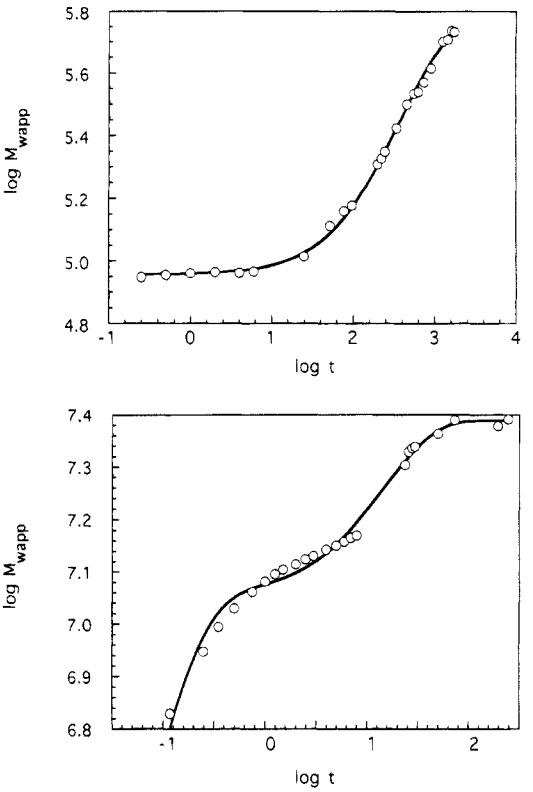

Figure 11. Examples of fitting curves for micellization: (a) eq 7 for KT-326 [$C = 0.600 \times 10^{-3}$ g (g of solution)$^{-1}$; $T = 15$ °C]; (b) eq 6 for KT-327 [$C = 5.934 \times 10^{-4}$ g (g of solution)$^{-1}$; $T = 35$ °C].

Table 2. Temperature Dependence of Relaxation Times for Micelle Formation of KT-327 at $c = 4.2874 \times 10^{-4}$ g (g of solution)$^{-1}$

temp, °C	$M_m - M_u$, $\times 10^{-6}$	m_1	τ_1, h	τ_2, h
45	32.1	0.412	0.0845	6.57
35	26.3	0.477	0.299	36.7
24	16.7	0.452	0.459	50.2
15	8.75	0.309	0.448	20.4

Table 3. Concentration Dependence of Relaxation Times for Micelle Formation of KT-327 at 35 °C

concn, $\times 10^4$ g (g of solution)$^{-1}$	$M_m - M_u$, $\times 10^{-6}$	m_1	τ_1, h	τ_2, h
8.142	23.9	0.589	0.0958	57.5
5.934	24.5	0.460	0.145	20.1
4.287	26.3	0.477	0.299	36.8
2.109	21.6	0.512	1.39	43.6

Table 4. Concentration Dependence of Relaxation Times for Micelle Formation of KT-326 at 15 °C

concn $\times 10^3$ g (g of solution)$^{-1}$	$M_m - M_u$, $\times 10^{-6}$	τ_1, h
1.517	2.56	23.5
1.200	2.08	42.8
0.808	0.878	217
0.601	0.490	737

reasonably good enough to evaluate representative time constants for the micellization processes. In Tables 2–4 are listed numerical values of the parameters obtained.

The time constants of the KT-327 system decrease with increasing temperature but are not so sensitive to temperature compared with concentration dependence. Concentration dependence of the time constants was plotted in double-logarithmic scale in Figure 12. The time constant τ_1 of the first process decreases with increasing polymer concentration, while τ_2 of the second process is almost independent of the concentration. The

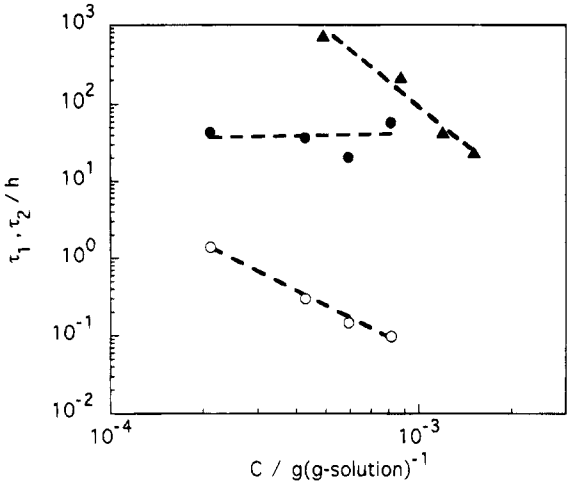

Figure 12. Log–log plots of τ_1 and τ_2 against the polymer concentration for KT-326 [τ_1 (▲)] and KT-327 [τ_1 (○); τ_2 (●)].

time constant τ_1 is much smaller than τ_2 by about 10^2 times, and the difference in rate between the two processes increases with increasing concentration owing to increasing rate of the first process. The first process of KT-326 is much slower than that of KT-327. Compared at $C = 4 \times 10^{-4}$ g (g of solution)$^{-1}$ and 15 °C, the difference is of the order of 10^3 times in terms of the time constant.

Conclusions

Micellization processes deduced here are schematically illustrated in Figure 13. The first process is formation of micelles with association number, P, being close to but not equal to the equilibrium one. The number of the micelles increases until the unimer concentration reaches a very low concentration around the critical micelle concentration. A characteristic feature of the first process is slow birth and quick growth of micelles, resulting in an increase in the number of micelles with similar sizes. In this sense, the process is similar to the nucleation and growth mechanism.

In the second process following the first process, the growth of the micelles is achieved by decomposition and growth of the micelles induced by expulsion and entry of unimers from/into micelles. This results in an increase of the association number and a decrease of the micelle number. The growth of micelle size must be relatively fast since the growth is made with excess unimers produced by the decomposition of vanished micelles. What results in the presence of the second process is that micelles formed in the first process are not equilibrium ones but quasi-equilibrium ones. A possible explanation for not reaching the equilibrium by a single step is this: Once the size of a micelle has exceeded a critical size, the micelle growth is fast initially but slows down very much when the micelle has grown to be a certain size close to the equilibrium size. Therefore, before growing micelles reach the equilibrium size, most of the free unimers have been consumed and the micellization has tentatively finished. This is the end of the first process, where the system has not reached the true equilibrium yet. The present result is consistent with the computer simulation of Mattice et al.,[24] which showed that the micellization occurs in two processes with different time scales: The volume fraction of free chains reaches its equilibrium value very quickly, which corresponds to the first fast

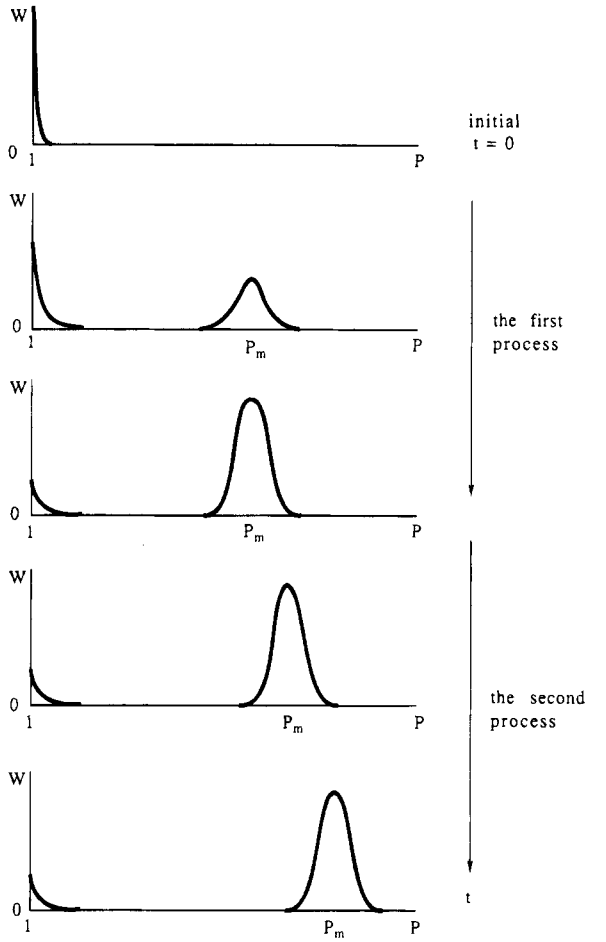

Figure 13. Schematic presentation of time variation of association number distribution in the course of the first and second micellization processes. Each peak has a finite width of the association number distribution. The association number P_m indicates a representative (i.e., the maximum) association number of micelles.

step of the present case, and the association number of the maximum size micelle converges at an intermediate rate, which corresponds to the second step.

As other mechanisms for the second process, one can generally suppose reorganization within respective micelles and fission–fusion of micelles. However, they are not likely in the present case. The increase of M_{wapp} in the second process indicates no reality of the reorganization without change of association number. Fission and fusion mechanisms are also less likely than the above-mentioned mechanism, because we observed no sign of increasing polydispersity during the course of the process, and it has been theoretically suggested that expulsion and entry of a polymer chain from/into the micelle can more easily occur than fission and fusion of micelles.[16,20] On the basis of the chain expulsion and entry processes, Tian et al. discussed kinetics of comicellization.[23]

The micellization mechanism proposed here is similar to that of the Aniansson–Wall theory[27] for aqueous amphiphilics in the senses that the micellization proceeds stepwise and that the entry and expulsion of unimers are elemental processes. The difference arises from the starting solution in the present case, which has no micelle but only unimers, being far from an equilibrium state, whereas the theory is for the relaxation processes near equilibrium. This gives rise to a difference between the fast process near the equilibrium and the first process observed here. The fast process

near the equilibrium is characterized by no essential change of the number of micelles, whereas the first process of the present case involves the increase of micelle number because new micelles can be produced since there exist many excess unimers at the early stage of the first process. The essential feature is, however, common that only the unimers can promote the process by entering into micelles without decomposition of once-formed micelles. In the second slow process, by exchanging unimers among micelles, some micelles decompose while other micelles increase their association numbers.

The rate-determining step in the first process is assembly of the unimers to make "associates of a critical size", i.e., birth of new micelles. Therefore, the rate of the first process may depend on the unimer concentration. On the other hand, the second process requires decomposition of micelles formed in the first process, and this decomposition may determine the rate of the second process, as long as the unimer concentration is not extremely low. These speculations on the concentration dependence of the rates of micellization processes are exactly what have been observed in the present study.

The decrease of time constants τ of KT-327 with increasing temperature is consistent with the results for aqueous amphiphiles.[31,33,35,38] In the present case, thermodynamical stability of micelles must decrease as temperature increases to approach the critical micellization temperature and may reduce the rate of micellization. However, in reality, the rate ($1/\tau$) increased with increasing temperature. This may suggest that increase in mobility of molecular motions with increasing temperature is more effective than change of the thermodynamical stability in the temperature dependence of τ.

Appendix: Variations of Apparent Quantities, M_{wapp}, R_{gapp}, and R_{happ}, Measured by Light Scattering in the Course of the Micelle Fraction Growth (the First Process) and the Micelle Size Growth (the Second Process)

We will here predict changes of the quantities M_{wapp}, R_{gapp}, and R_{happ}, which are measured by light scattering, in the micellization process for extreme cases, to distinguish which is the dominant process—the micelle fraction change or the micelle size change. The idea for distinction of the process is based on the fact that M_{wapp} is primarily determined by the molecular weight and the fraction of micelle-forming copolymers, while R_{gapp} and R_{happ} are dominated by the size of large particles, i.e., micelles; in other words, each of these three quantities reflects the association number and the total number of micelles in the solution in different way from the others.

Consider a solution of block copolymer forming closed micelles in selective solvent. Then the system we are concerned with is considered to generally consist of micelles with a certain association number and unimers in solvent, as in the case of the model represented in Figure 13 under the approximation of monodisperse distribution of P for peaks around unimers and micelles. Variables are the molar mass of a micelle and the weight fraction of micelle-forming copolymer in the total polymer, being denoted M_m and w_m, respectively. The extreme cases are described with these quantities, for instance, as follows: In the case of the fraction growth process, M_m is constant, whereas w_m is variable, changing from zero to unity. On the other hand, in the case of the size growth process, M_m is increasing, with w_m being fixed at unity.

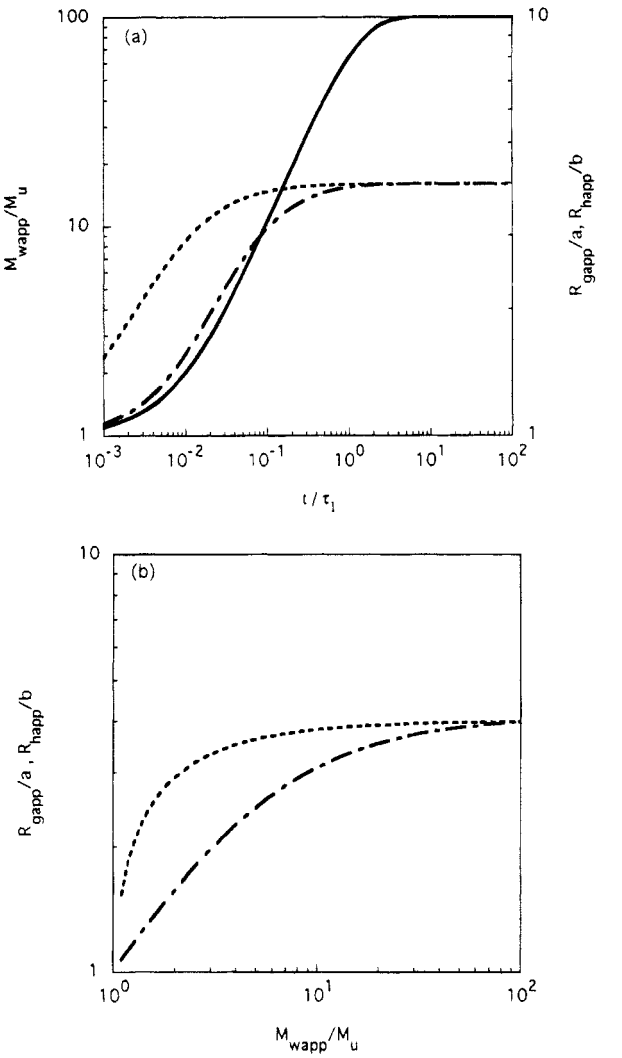

Figure A1. Calculated curves of M_{wapp}/M_u, R_{gapp}/a, and Rh_{app}/b vs t/τ_1 and of R_{gapp}/a and R_{happ}/b vs M_{wapp}/M_u for case 1: (a) M_{wapp}/M_u (solid line); R_{gapp}/a (dashed line); R_{happ}/b (dot-dash line). (b) R_{gapp}/a (dashed line); R_{happ}/b (dot-dash line).

In considering the quantities measured by light scattering, we have to approximate the solution to be infinitely dilute. This may be a crucial approximation, but there is no way to avoid it due to the nature of the experiments. Discrepancy from the real dilute limit may hopefully be of almost the same degree in all cases considered here, and if so, the approximation is not so bad, as long as we are not concerned with absolute values of micelle sizes.

Under the dilute-limit approximation, M_{wapp} is the weight average molecular weight of the system. M_{wapp} is expressed as

$$M_{wapp} = M_m w_m + M_u w_u \tag{A1}$$

where M_u and w_u (=1 − w_m) are the molar mass and weight fraction of the unimer, respectively. ${R_{gapp}}^2$ is the z-average of ${R_g}^2$, and therefore one has

$${R_{gapp}}^2 = {R_{gm}}^2 z_m + {R_{gu}}^2 z_u \tag{A2}$$

with

$$z_m = M_m w_m / M_{wapp} \tag{A3}$$

$$z_u = M_u w_u / M_{wapp} \tag{A4}$$

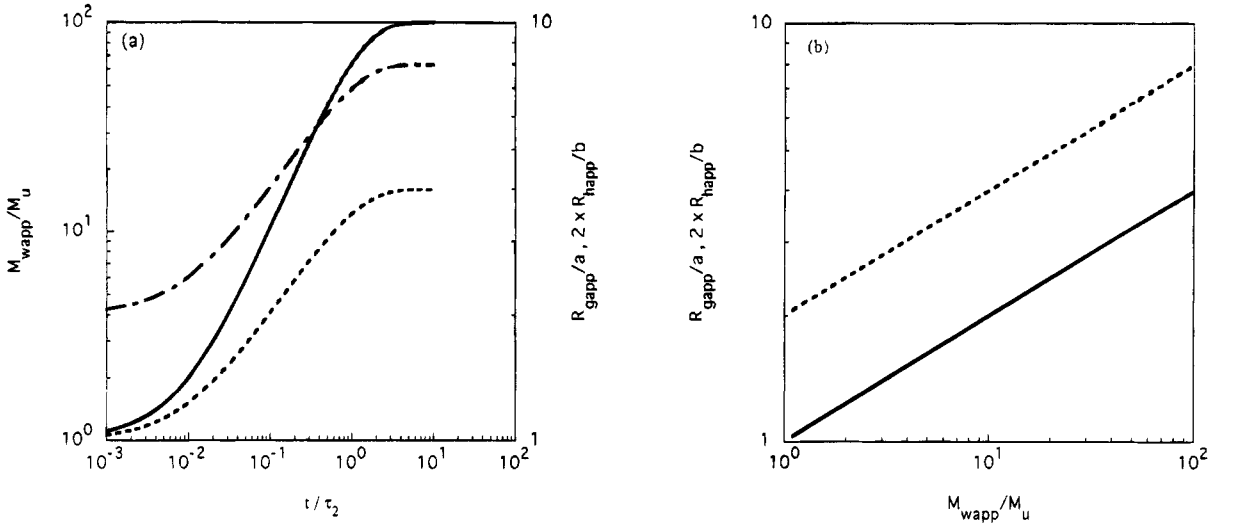

Figure A2. Calculated curves of M_{wapp}/M_u, R_{gapp}/a, and $2R_{happ}/b$ vs t/τ_2 and of R_{gapp}/a and $2R_{happ}/b$ vs M_{wapp}/M_u for case 2: (a) M_{wapp}/M_u (solid line); R_{gapp}/a (dashed line); $2R_{happ}/b$ (dot-dash line). (b) R_{gapp}/a (solid line); $2R_{happ}/b$ (dashed line).

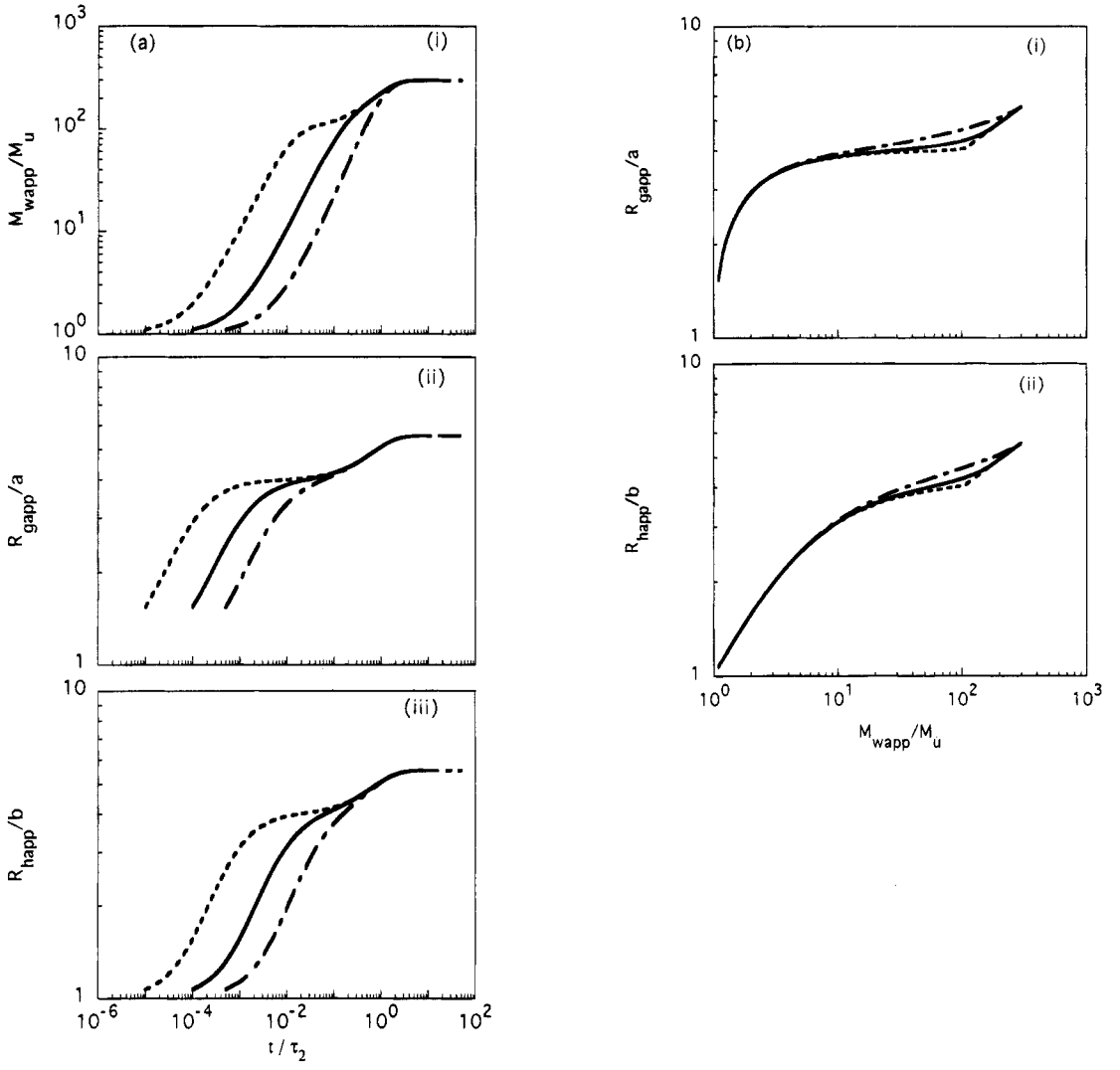

Figure A3. Calculated curves of M_{wapp}/M_u, R_{gapp}/a, and R_{happ}/b vs t/τ_2 and of R_{gapp}/a and R_{happ}/b vs M_{wapp}/M_u for case 3 of $\tau_1/\tau_2 = 0.5$ (dot-dash line), 0.1 (solid line), and 0.01 (dashed line): (a) (i) M_{wapp}/M_u, (ii) R_{gapp}/a, (iii) R_{happ}/b; (b) (i) R_{gapp}/a, (ii) R_{happ}/b.

R_{happ} obtained with the cumulant method from the correlation function measured at the wavenumber q is given by

$$(R_{happ})^{-1} = {R_{hm}}^{-1}s_m + {R_{hu}}^{-1}s_u \qquad \text{(A5)}$$

Here, the weights s_m and s_u are those of the intensity $I(q)$ of scattered light at q from the components m and u, respectively, which can be calculated by the following approximated expressions for scattered light intensity of each component:

$$I_m(q) = M_m w_m/(1 + q^2{R_{gm}}^2/3) \qquad \text{(A6)}$$

$$I_u(q) = M_u w_u/(1 + q^2{R_{gu}}^2/3) \qquad \text{(A7)}$$

Then

$$s_m = I_m(q)/[I_m(q) + I_u(q)] \quad \text{(A8)}$$

$$s_u = I_u(q)/[I_m(q) + I_u(q)] \quad \text{(A9)}$$

For the following extreme cases 1 and 2, and their combination, case 3, predicted M_{wapp}, R_{gapp}, and R_{happ} were calculated using eqs A3, A4, and A5.

case 1, fraction growth process

$$M_m = M_{m0};\ w_m = 1 - \exp(-t/\tau_1) \quad \text{(A10)}$$

case 2, size growth process

$$M_m = M_u + (M_{m0} - M_u)[1 - \exp(-t/\tau_2)];\quad w_m = 1 \quad \text{(A11)}$$

case 3, stepwise growth

$$M_m = M_{m0} + (M_{m1} - M_{m0})[1 - \exp(-t/\tau_2)];\quad w_m = 1 - \exp(-t/\tau_1) \quad \text{(A12)}$$

with $\tau_1 < \tau_2$. Equation A11 yields eq 7 of M_{wapp} in the case of $\tau_1 \ll \tau_2$. In the calculations, equations for R_g and R_h as functions of molar mass M_m were needed, which were put as

$$R_g(M) = a(M/M_u)^\nu \quad \text{(A13)}$$

$$R_h(M) = b(M/M_u)^\nu \quad \text{(A14)}$$

with the exponent ν being 0.3.[40] Qualitative results of the calculation were not sensitive to the value of ν. The calculated results are presented as log–log plots of M_{wapp}/M_u, R_{gapp}/a, and R_{happ}/b vs t/τ_1 or t/τ_2 and of R_{gapp}/a and R_{happ}/b vs M_{wapp}/M_u for cases 1, 2, and 3 in Figures A1, A2, and A3, respectively. Here we put $M_{m0}/M_u = 100$ and $M_{m1}/M_{m0} = 3$. The value of a, which was needed for evaluating the intensity $I(q)$ by eq A6, was chosen such that eq A6 described the R_{gapp} vs M_{wapp} relation for M_{wapp} greater than 3×10^6 g mol^{-1}, i.e., $a = 4.724 \times 10^{-9}$ m. The wavenumber q was taken to be that of the present experiments. The term $q^2R_{gm}^2/3$ in eq A6 had only subtle effects on the results of calculation.

In the calculated curves of case 1, R_{gapp} approaches R_{gm} earlier than M_{wapp} becomes close to M_m, exhibiting the characteristic shape of the log R_{gapp} vs log M_{wapp} curve similar to that of the first process observed in this study. In case 2, the parallel growth of R_{gapp} and M_{wapp} is obtained as seen in the second process of KT-327. Case 3 of stepwise micellization reproduces the experimental characteristic features of time evolution of M_{wapp} and R_{gapp}, although in reality the stepwise changes are less discrete, with broader distributions of time constant.

References and Notes

(1) Tuzer, Z.; Kratochvil, P. *Surface Colloid Sci.* **1993**, *15*, 1.
(2) Noolandi, J.; Hong, K. M. *Macromolecules* **1983**, *16*, 1443.
(3) Leibler, L.; Orland, H.; Wheeler, J. C. *J. Chem. Phys.* **1983**, *79*, 3550.
(4) Whitmore, M. D.; Noolandi, J. *Macromolecules* **1985**, *18*, 657.
(5) Roe, R-J. *Macromolecules* **1986**, *19*, 728.
(6) Halperin, A. *Macromolecules* **1987**, *20*, 2943.
(7) Marques, C.; Joanny, J. F.; Leibler, L. *Macromolecules* **1988**, *21*, 1051.
(8) Nagarajan, R.; Ganesh, K. *J. Chem. Phys.* **1989**, *90*, 5843.
(9) Leibler, L. *Physica A* **1991**, *172*, 258.
(10) Shim, D. F. K.; Marques, C.; Cate, M. E. *Macromolecules* **1991**, *24*, 5309.
(11) Yuan, X.-F.; Masters, A. J.; Price, C. *Macromolecules* **1992**, *25*, 6876.
(12) Zhou, Z.; Chu, B. *J. Interface Sci.* **1988**, *126*, 171.
(13) Zhou, Z.; Chu, B. *Macromolecules* **1988**, *21*, 2548.
(14) Bednar, B.; Edwards, K.; Almgren, M.; Tormod, S.; Tuzar, Z. *Makromol. Chem., Rapid Commun.* **1988**, *9*, 785.
(15) Halperin, A.; Alexander, S. *Europhys. Lett.* **1988**, *6*, 329.
(16) Halperin, A.; Alexander, S. *Macromolecules* **1989**, *22*, 2403.
(17) Hilfiker, R.; Chu, B.; Xu, Z. *J. Colloid Interface Sci.* **1989**, *133*, 176.
(18) Tsunashima, Y. *Macromolecules* **1990**, *23*, 2963.
(19) Xu, R.; Winnik, M. A.; Riuss, G.; Chu, B.; Croucher, M. D. *Macromolecules* **1992**, *25*, 644.
(20) Halperin, A.; Tirrell, M.; Lodge, T. P. *Adv. Polym. Sci.* **1992**, *100*, 31.
(21) Zhou, Z.; Chu, B.; Peiffer, D. G. *Macromolecules* **1993**, *26*, 1876.
(22) Mortensen, K.; Brown, W. *Macromolecules* **1993**, *26*, 4128.
(23) Tian, M.; Qin, A.; Ramireddy, C.; Webber, S. E.; Munk, P.; Tuzar, Z.; Prochazka, K. *Langmuir* **1993**, *9*, 1741.
(24) Wang, Y.; Mattice, W. L.; Napper, D. H. *Langmuir* **1993**, *9*, 66.
(25) Quintana, J. R.; Villacampa, M.; Katime, I. A. *Macromolecules* **1993**, *26*, 601.
(26) Muller, N. *J. Phys. Chem.* **1972**, *21*, 3017.
(27) Aniansson, E. A. G.; Wall, S. N. *J. Phys. Chem.* **1974**, *78*, 1024.
(28) Nakagawa, T. *Colloid Polym. Sci.* **1974**, *252*, 56.
(29) Aniansson, E. A. G.; Wall, S. N. *J. Phys. Chem.* **1975**, *79*, 857.
(30) Lang, J.; Tondre, C.; Zana, R.; Bauer, R.; Hoffmann, H.; Ulbricht, W. *J. Phys. Chem.* **1975**, *79*, 276.
(31) Aniansson, E. A. G.; Wall, S. N.; Almgren, M.; Hoffmann, H.; Kielmann, I.; Ulbricht, W.; Zana, R.; Lang, J.; Tondre, C. *J. Phys. Chem.* **1976**, *80*, 905.
(32) Kahlweit, M.; Teubner, M. *Adv. Colloid Interface Sci.* **1980**, *13*, 1.
(33) Lessner, E.; Teubner, M.; Kahlwelt, M. *J. Phys. Chem.* **1981**, *85*, 1529.
(34) Lessner, E.; Teubner, M.; Kahlwelt, M. *J. Phys. Chem.* **1981**, *85*, 3167.
(35) Kahlweit, M. *J. Colloid Interface Sci.* **1982**, *90*, 92.
(36) Aniansson, E. A. G. In *Aggregation Processes in Solution*; Wyn-Jones, E., Gormally, J., Eds.; Elsevier: Amsterdam, 1983; Vol. 26, p 70.
(37) Kahlweit, M. In *Physics of Amphiphiles: Micelles Vesicles and Microemulsions*; Degiorgio, V., Corti, M., Eds.; North-Holland: Amsterdam, 1985; p 212.
(38) Lang, L.; Zana, R. In *Surfactant Solutions*; Surfactant Science Series; Zana, R., Ed.; Dekker: New York, 1986; Vol. 22, p 405.
(39) Hirao, A.; Yamamoto, A.; Takenaka, K.; Yamaguchi, K.; Nakahama, S. *Polymer* **1987**, *28*, 303.
(40) Honda, C.; Sakaki, K.; Nose, T. *Polymer* **1994**, in press.
(41) Pike, E. R.; Pomeroy, W. R. M.; Vaughan, J. M. *J. Chem. Phys.* **1975**, *62*, 3188.
(42) Koppel, D. E. *J. Chem. Phys.* **1972**, *57*, 4814.